SolarPACES 2024, 30th International Conference on Concentrating Solar Power, Thermal, and Chemical Energy Systems

Power Cycles

https://doi.org/10.52825/solarpaces.v3i.2414

Published: 22 Oct. 2025

Effect of Compressor Inlet Swirl on Solar Gas Turbine Performance

Matthew R. Meas[1,*], Sybrand J. van der Spuy[1], and Andrew Gill[1]

[1]Solar Thermal Energy Research Group, Stellenbosch University, Private Bag X1, Matieland 7602, Stellenbosch, South Africa

*Correspondence: Matthew Robert Meas, mmeas@sun.ac.za

Abstract. An investigation of the effect of various compressor inlet guide vane (IGV) setting angles on the thermodynamic performance of a simple single shaft solar-hybrid gas turbine power generation system (SHGT) is presented. The formulation of models for the individual system components is described, with emphasis on the generation of compressor characteristics for various IGV setting angles. Matching of the components in the integrated system model is shown, for the standard single shaft turboshaft configuration as well as several variable rotor speed turboshaft configurations. The estimated fuel consumption, solar receiver effectiveness, and thermal efficiency are compared for the reference system, SHGTs with IGVs, and variable rotor speed SHGT configurations. The results of the performance calculations for a 40 kW_e gas turbine engine indicate that a 4.3 % reduction in full-load fuel consumption is attainable with compressor IGVs set at 9° in the direction of the rotor blade rotation, and a reduction of 25.3 % is attainable with independent and distinct compressor and turbine rotor speeds.

Keywords: Solar Gas Turbine, Inlet Guide Vanes, Swirl

1. Introduction

The integral “spool” assembly formed by the compressor, turbine and connecting shaft of the conventional gas turbine engine core has been a quintessential feature of the technology since its invention nearly one hundred years ago. The fixed physical linkage between the turbine and compressor rotors reduces complexity, and therefore manufacturing- and maintenance costs, all of which contribute to the prevalence of the technology. However, the conventional common shaft arrangement also imposes operational constraints, the significance of which depends on the application in which the engine is deployed. These constraints, as they apply to solar hybrid gas turbine (SHGT) systems, are discussed in a previous paper by the authors [1] in which an approach to overcoming their effects is proposed and analysed, which involves various modifications to the systems to permit variable rotor speeds. In this present paper, another approach to improving component matching in SHGT systems is considered, which entails using compressor inlet guide vanes (IGVs). Further development in the investigation of variable rotor speed SHGT configurations is also discussed. A synopsis of the thermofluid dynamics of turbomachines is first presented, in which the constraints on the component matching in conventional gas turbines are illustrated, and the ideas that bely the potential solutions are explained. The methods and scope of analysis are then described, and the performance that is estimated to be attainable if compressor IGVs are used to facilitate improved component matching in SHGT systems is compared to that estimated for an SHGT system without compressor IGVs and various SHGT systems designed for variable rotor speeds.

2. Component matching in solar gas turbines

Energy transfer in turbomachines occurs due to dynamic interaction between the working fluid and the rotor blades. By considering the velocity of the rotor blades, U, and that of the fluid, C, the rate of energy transfer may be calculated using the Euler turbomachinery equation (Equation 1), enabling the corresponding changes in temperature and pressure in the rotor section to be determined.

$$\Delta W = h_{01} - h_{02} = U_1 \cdot C_{\theta 1} - U_2 \cdot C_{\theta 2} \quad (1)$$

Adjusting the blade- or fluid velocity at the inlet or outlet of the rotor alters the rate of energy transfer in the machine. The extent of the change depends on the relative proportions of the velocities. Modifying the geometry of a component in a turbomachine causes the direction of the fluid velocity and the proportions of the related velocity triangle to change, altering the very manner in which changes in the velocity magnitudes affect the performance of the machine, transforming its characteristic maps.

When multiple turbomachines are connected, as in a gas turbine engine, interactions between the characteristics of the turbomachines must be considered, as well as interactions with other components installed in the fluid circuit, such as combustors, recuperators, or solar receivers. For a single shaft gas turbine operating at a specified absolute running speed, every unique value for the turbine inlet temperature (TIT) prescribes a corresponding line of constant corrected speed on the turbine characteristic. For any point on the line of constant speed on the compressor characteristic, the corresponding values of the turbine pressure ratio and corrected mass flow rate can be computed. However, due to the converse shapes of the speed lines on the compressor and turbine maps, the operating conditions of the compressor and turbine are compatible at only one point on the compressor speed line for a given TIT. At the other points on the compressor speed line, the incompatibility of the turbine and compressor may be conceptualised as follows: for the corrected mass flow rate and corrected speed corresponding to the compressor operating point, the value for the turbine pressure ratio that is indicated by the turbine characteristic map may differ from the value that is physically dictated by compressor pressure ratio, or vice versa. For a specified running speed and TIT, the attainable net power output is the difference between the turbine power output and the compressor power consumption at the matched compressor and turbine operating points determined in this manner. Should it be necessary to adjust the net power output whilst maintaining a prescribed running speed, the TIT must be adjusted and a new of matched operating point established as just described. If the number of running speeds is increased, the number of compatible operating points on the compressor and turbine characteristics can theoretically be increased proportionally, depending on the characteristics of the individual turbomachines and the required load. Independent and distinct rotor speeds should theoretically increase the number of compatible operating points further still, as for every compressor operating point, it would then be possible to vary the turbine corrected speed- and mass flow rate values by changing both the TIT and the absolute speed of the turbine rotor independently of the compressor rotor speed.

Alternatively, the geometry of components of the turbomachines may be varied, as previously described. This can be accomplished using devices such as compressor IGVs, variable diffuser vanes, and variable turbine nozzles, which are commonly used for controlling local flow conditions in turbomachines to avoid formation of shock waves. The selection of compressor IGVs from the options available for consideration in this work is motivated by the practical appeal of the relative ease with which IGVs may be retrofitted to the compressor of an existing gas turbine engine.

3. Modelling

The arrangement of the compressor, solar receiver, combustor, and turbine in the reference SHGT system is shown in Figure 1. The other SHGT configurations considered in this analysis differ only by the incorporation of compressor IGVs, or auxiliary components attached to the shafts connecting the compressor, turbine, and generator. More information on these cases is given in the discussion of the performance calculations in section 4. This section describes the thermodynamic modelling of the components that comprise the SHGT systems.

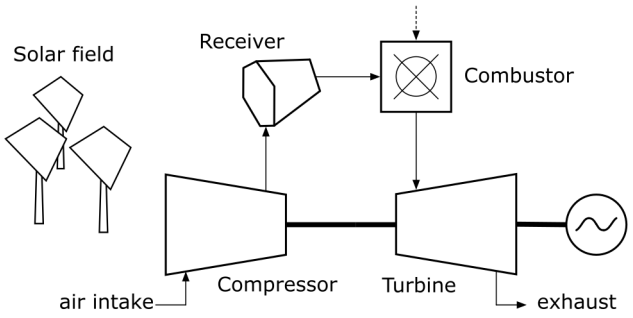

***Figure 1**. Reference solar hybrid gas turbine configuration.*

3.1 Turbomachinery

The precise way in which compressor characteristics are transformed by the presence of inlet swirl is dependent on the design of the machine. Due to the limited availability of complete design data in the literature, a comprehensive analysis supported by information on multiple gas turbines is beyond the scope of this work. Instead, the investigation considers the Rover 1S/60 gas turbine, an example of which is retained and operated at Stellenbosch University, and for which a 3D model of the compressor has been created [2]. The design data for the Rover 1S/60 engine are shown in Table 1.

***Table 1**. Design point performance specifications of the Rover 1S/60 gas turbine.*

Net power output [kW]	45
Mass flow rate [kg/s]	0.6
Engine pressure ratio (p_{02}/p_{01})	2.8
Overall thermal efficiency ($\eta_{TT,0\text{-}4}$)	0.10
Rotational speed [RPM]	46000
Compressor isentropic efficiency	0.70
Turbine isentropic efficiency	0.85
Combustor efficiency	0.99
Maximum turbine inlet temperature [K]	1023

3.1.1 Compressor

The one-dimensional analyses developed by Aungier [3] permit estimates for the performance of the components of a centrifugal compressor to be made under different conditions, given basic geometric data and their design point performance specifications. For this work, an internally developed code [4] in which these analyses are implemented is used to generate characteristic maps for the centrifugal compressor of the Rover 1S/60 gas turbine engine.

The inlet guide vane performance analysis employs basic empirical models to compute the discharge flow angle and the total pressure loss coefficient for the blade row, requiring only the mean radii and blade angles, meridional length and cross-sectional areas of the blade

passages, and the number of vanes to be specified. The computed values of the flow conditions at the outlet of the blade row are supplied to the impeller analysis as inlet conditions, the outlet conditions of which are then supplied as inputs to the performance analysis of the vaneless annular passage, and so forth. For simplicity, this work assumes a symmetric vane profile. In the impeller performance analysis, the blade work input is computed for assumed values of the isentropic total relative discharge flow conditions, following an approach similar to that described in section 2, above. The loss coefficients needed to account for the various total pressure losses in the impeller are subsequently computed and used to estimate the actual relative discharge flow conditions. The process is repeated until converged values are obtained for the discharge relative flow conditions and the corresponding flow coefficient, at which point the absolute flow conditions may be computed using the definitions for the impeller work input factor and rothalpy. The performance analysis of the vaneless annular passage is based on a set of governing equations for one-dimensional free vortex flow in a vaneless passage with losses due to wall friction, passage curvature, and flow diffusion. Solving the finite difference forms of these governing equations using a forward marching algorithm proceeding from the inlet boundary yields the flow conditions at the outlet. In the vaned diffuser performance analysis, the cumulative total pressure loss is estimated for assumed values of the discharge flow conditions, using an approach similar to that used in the impeller performance analysis. The discharge flow angle is then computed using correlations similar to those employed in the IGV analysis. The discharge static pressure and density are then updated using the computed total discharge pressure, and used, together with the mass flow rate and the computed discharge flow angle, to obtain updated values for the discharge velocity components. The solution proceeds iteratively until a converged value is obtained for the discharge meridional velocity, after which the overall pressure ratio and isentropic efficiency of the compressor is computed.

The characteristic maps for the compressor are generated by repeating these one-dimensional performance analyses for a range of mass flow rates, and multiple impeller running speeds. Since the analyses do not yield precise estimates for the mass flow rate values corresponding to the onset of stall or choking in the blade passages, these are defined with simple heuristics. For each speed line, the inflection points of the total-to-total- and total-to-static pressure ratio characteristic are determined, and the greater value regarded as the surge limit. The choke limit for each speed line is defined as the mass flow rate value above which a predetermined incremental increase in the mass flow rate causes a drop in the isentropic efficiency of the compressor greater than 5 %. Since the nominal mass flow rate of the Rover 1S/60 is less than 1 kg/s, the incremental mass flow rate increase considered is 0.0001 kg/s.

For this work, characteristic maps are generated for IGV setting angles, relative to the axial direction, ranging from -9° to 9° in increments of 3°. The maps generated for IGV setting angles of -9°, 0°, and 9° are shown, superimposed, in Figure 2. The maps are employed in the solution algorithms devised for carrying out the SHGT system performance calculations in the form of two-dimensional spline objects. Since the mass flow rate limits differ for each speed line, the characteristic data for each speed line, including the mass flow rate, is defined at a prescribed number of points, and the corresponding spline objects defined in terms of the relative corrected speed and non-dimensional coordinate along the speed line, β. The compressor characteristics may thus be quickly retrieved at any operating point, specified by these two parameters, and the calculations needed to determine the thermodynamic flow conditions at the compressor discharge carried out using basic relations for isentropic flow.

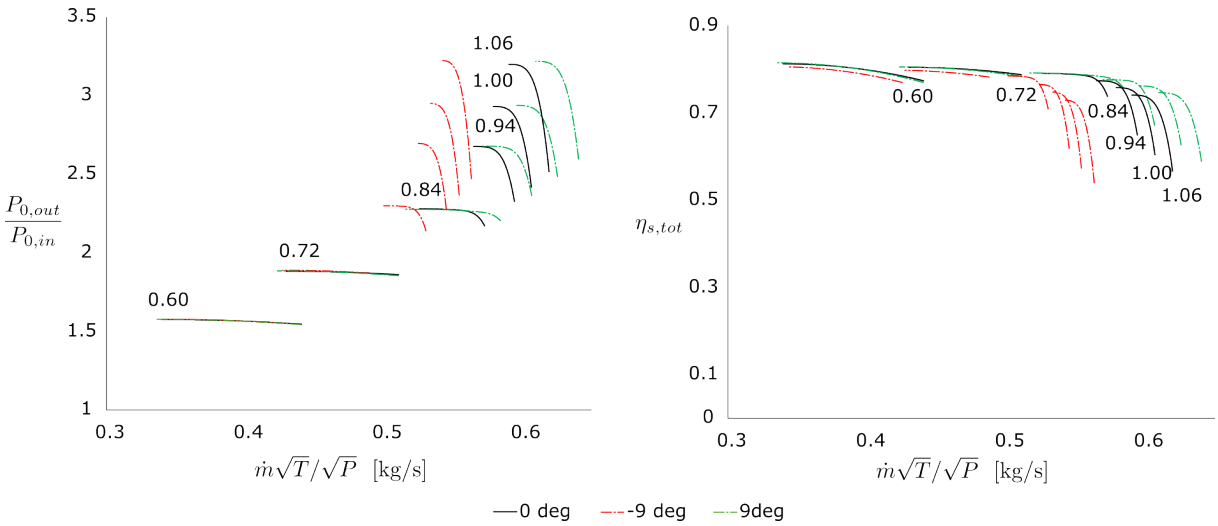

Figure 2. *Pressure ratio and efficiency characteristics of the centrifugal compressor of the Rover 1S/60 gas turbine engine for various inlet guide vane setting angles.*

3.1.2 Turbine

The turbine is modelled much like the compressor, using isentropic flow relations and characteristic data stored in spline objects to determine the values of the applicable unknown flow conditions. The characteristic data for the single stage axial flow turbine of the Rover 1S/60 gas turbine engine are not known to have been published, nor have geometric data been acquired for the turbine. Approximate characteristic maps are therefore generated by using the map scaling feature of the software package GasTurb [5] to match the characteristic maps of a similar turbine to the design point performance specifications of the turbine of the Rover 1S/60. The characteristic maps selected for this purpose are those of the NASA-CR-174646 variable geometry turbine, taken from the collection of maps included with GasTurb 14.

3.2 Combustor

Combustion energy usage in the SHGT systems is computed using the basic energy balance equation for adiabatic combustion with no work transfer. Expanding the energy balance, making use of the enthalpy of reaction at a reference temperature of 298 K, Equation 2 is obtained, where c_{pg} denotes the specific heat capacity of the combustion products evaluated at the average of the reference- and outlet temperatures, c_{pf} and c_{pa} denote the specific heat capacities of the air and fluid streams respectively at their analogous average temperatures, and f denotes the fuel-air ratio [6]. For this work, a typical lower heating value for kerosene (LHV = 43.1 MJ/kg), the prescribed fuel for the Rover 1S/60, is considered. In the solution algorithms, described in section 4 below, Equation 2 is rearranged to facilitate the computation of the fuel-air ratio and the corresponding fuel mass flow rate needed to attain a set temperature at the turbine inlet.

$$(1+f)\cdot c_{pg}\cdot(T_{out}-298)+f\cdot \mathrm{LHV}+c_{pa}\cdot(298-T_{in})+f\cdot c_{pf}\cdot\left(298-T_f\right)=0 \qquad (2)$$

A total pressure drop equal to 5 % of the total pressure at the combustor inlet is applied across the combustor in the performance calculations. This chosen value is the average of the typical range noted by Saravanamuttoo et al. (6-8 % for aero-engines, and 2-3 % for large industrial units with correspondingly low combustor flow velocities) [6].

3.3 Solar receiver

A simple thermodynamic model for a single open-cavity pressurised air receiver positioned at the focal point of a polar heliostat field is employed for consideration of the solar thermal energy

utilisation in the SHGT systems. The heat losses by thermal radiation and mixed convection through the receiver aperture, and forced convection from the insulated exterior walls, is subtracted from the solar flux reflected onto the receiver aperture to determine the rate of heat transfer to the air flowing through the absorber tube, per the following energy balance:

$$\dot{Q}_{sol} + \dot{Q}_{loss,conv} + \dot{Q}_{loss,rad} + \dot{Q}_{abs} = 0 \quad (3)$$

The solar flux reflected onto the receiver aperture is calculated using the equation

$$\dot{Q}_{sol} = \eta_{opt} \cdot A_{field} \cdot \mathrm{DNI} \quad (4)$$

where the empirical correlation

$$\eta_{opt} = 0.4245 \cdot \theta_z^6 - 1.148 \cdot \theta_z^5 + 0.3507 \cdot \theta_z^4 + 0.755 \cdot \theta_z^3 - 0.5918 \cdot \theta_z^2 + 0.0816 \cdot \theta_z + 0.832 \quad (5)$$

derived by Gauche et al. [7] is used to estimate the optical efficiency of the heliostat field and cavity receiver given the solar zenith angle at the applicable time of day and plant location, as computed using the algorithm described by Stine and Harrigan [8]. The concentrated flux is assumed to be distributed uniformly on the absorber tube.

As described by le Roux [9], the convective heat losses from the receiver cavity are determined using the Koenig and Marvin heat loss model, the convective heat losses from the exterior receiver walls are determined using standard one-dimensional correlations for combined laminar and turbulent parallel- and crossed flow past flat plates, and the quartic temperature terms in the radiative heat transfer equation are linearised using linear regression across the applicable temperature range. An average surface emissivity of 0.2 is used, as well as a wind factor of 2 for an assumed wind speed of 2.5 m/s, and the receiver is assumed to have an inclination of 45°. The internal forced convection is calculated using the Gnielinsky and Colebrook equations to determine the Nusselt number and Darcy-Weisbach friction factor, assuming a surface roughness of 0.002 mm in the absorber tube. The total pressure drop in the absorber tube is determined using the definition of the Darcy-Weisbach friction factor:

$$\Delta p = f_i \cdot \frac{L}{d_i} \cdot \frac{\rho \cdot \bar{U}^2}{2} \quad (6)$$

The expanded energy equation is solved iteratively to obtain the average surface temperature of the absorber tube and the temperature of the air at the outlet of the absorber tube. The design specifications of the heliostat field and receiver listed in Table 2 are used in this work, as they are permit a design solar fraction of approximately 60 %.

Table 2. *Design specifications for the solar collector and receiver.*

Heliostat field area [m^2]	400
Receiver aperture area [m^2]	0.115
Receiver tube diameter [m]	0.1
Receiver tube length [m]	15

4. Performance calculations

4.1 Cases

Performance calculations are carried out for five cases altogether - a SHGT system with IGVs, a reference configuration, and the three variable rotor speed configurations depicted in Figure 3, for comparison. Detailed descriptions of the latter configurations, and an analysis of their relative merits are presented in [1]. In the first variable rotor speed configuration, power electronics are used to enable the running speed of the turboshaft to be varied without interrupting the synchronisation of the generator output with the electrical grid. In the second, the nominal

turbine speed is maintained, and a variator is used to alter the speed at which power is supplied to the compressor. The third variable rotor speed configuration combines the power electronics and variator to allow the turbine and compressor to run at distinct speeds. All calculations assume a permanent magnet synchronous generator, negating the need to specify a torque-speed characteristic.

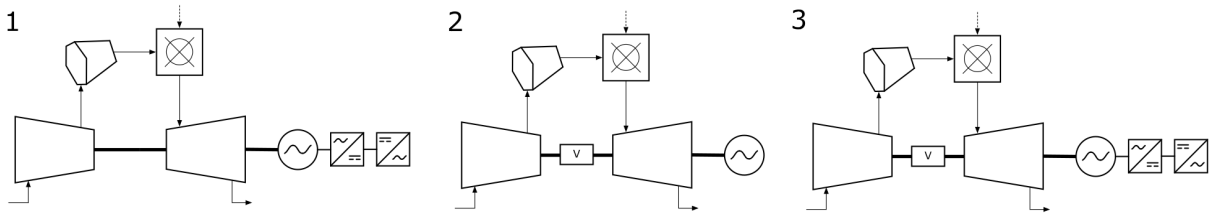

Figure 3. *Variable rotor speed solar hybrid gas turbine configurations.*

4.2 Solution algorithms

The solution algorithm for each case consists of four subroutines, for carrying out the performance calculations for the compressor, solar receiver, turbine, and combustor, in this specific sequence. The subroutines which carry out the compressor and the turbine performance calculations may take on one of two forms, depending on whether the running speed of the machine is to be specified or calculated. As some of the configurations differ only in their applicable input values, there are three unique solution algorithms for the five cases. For brevity, a description of the most pertinent variant – that applicable to the reference case and the SHGT with compressor IGVs - is presented here. The sequence of operations in the solution algorithm is as follows:

1. Compressor subroutine
   1.1. The relative corrected speed is specified for the compressor, and the spline objects for the compressor characteristics are evaluated at the corresponding rotor speed value, for multiple values of the non-dimensional length, β. This yields an array of operating points, each consisting of a mass flow rate, pressure ratio, and isentropic efficiency value.
   1.2. The first operating point in the array is then selected.
   1.3. With the mass flow rate, pressure ratio, and isentropic efficiency thus defined, the compressor discharge temperature and power consumption are computed.

2. Receiver subroutine
   The receiver calculations described in section 3.3 are carried out to compute the rate of thermal energy absorption in the receiver and the corresponding temperature rise and pressure drop across the receiver, using the mass flow rate and operating pressure determined in the preceding step.

3. Turbine subroutine
   3.1. The first (lowest) value in the array of the relative corrected speeds for the turbine is selected.
   3.2. An attempt is made to compute the corrected turbine mass flow rate at which the turbine pressure ratio, evaluated at the specified relative corrected speed using the spline object for the turbine characteristic, would equal the actual ratio of the calculated receiver outlet pressure to the total pressure (ambient) at the turbine outlet. If the attempt is successful, the subroutine proceeds to the next step. If not, the next value in the speeds array is selected, and the attempts are repeated until a real corrected mass flow rate is determined. If no value is found when the final value in the speeds array has been considered, the algorithm proceeds to step 5.

3.3. Once a corrected mass flow rate value is found, it is used, along with the actual cycle mass flow rate, to determine the turbine inlet temperature (TIT) using the definition of the corrected mass flow rate.
3.4. The calculated TIT and the actual running speed (specified in the compressor subroutine) are used to check the value of the relative corrected speed, using the definition of the corrected speed. If the computed relative corrected speed is consistent with the value specified in the first operation in the sequence, the subroutine proceeds to the next step. If not, the next value in the speeds array is selected, and the subroutine returns to step 3.2. If no value is found when the final value in the speeds array has been considered, the algorithm proceeds to step 5.
3.5. Once a consistent turbine operating point has been determined, the turbine exhaust temperature and power output are computed.

4. Combustor subroutine
The rate of energy input and the associated rate of fuel consumption required to attain the calculated TIT are determined, along with the pressure drop in the combustor, as described in section 3.2.

5. Iteration
Steps 1.2 – 4 are attempted for each operating point in the array mentioned in step 1.1. For every successful calculation, the β-coordinate of the compressor operating point, and the calculated system net power output are appended to the list of input- and output values to be used in the subsequent optimisation step in the solution algorithm.

6. Optimisation
The power output values in the abovementioned list are compared against the target value, and the input β-value corresponding to the minimum difference between the calculated and target power output values is identified. A one-dimensional optimisation problem is then solved, using this β-value as the starting point, in which the difference between the calculated and target power output values is minimised. Matching of the system components is thus obtained.

The solution algorithms for the variable rotor speed SHGT configurations are largely similar, but with the subroutines for compressor and turbine, and the iteration and optimisation steps tailored to the applicable input parameters and the output parameters to be calculated.

5. Findings

Performance metrics, calculated for a prescribed load of 40 kW_e and solar irradiance of 1000 W/m^2, at solar noon, are collated in Table 3 for the SHGT configurations that exhibit the most notable differences relative to the reference system. The reduced load of 40 kW_e is used due to the increased pressure drop across the receiver and combustor compared to the pressure drop across the combustor alone in the unmodified Rover 1S/60 engine, which could cause the maximum turbine inlet temperature to be exceeded at the design load. The results for SHGTs with compressor IGVs show the 9° IGV setting angle to be most beneficial, causing estimated changes in the fuel mass flow rate and solar fraction, of -4.3 % and 1.2 %, respectively, relative to the reference case. The -9° IGV setting angle is shown to be most detrimental, with corresponding changes of 22.7 % and -5.7 %. Similar, less pronounced effects are seen in the results for IGV setting angles between these limits. In all cases, improvement in the efficiency of one of the turbomachines is accompanied by a decrease in that of the other.

Table 3. *Collated results of the performance calculations for selected solar hybrid gas turbine configurations for 40 kW_e net power output and 1000 W/m² solar irradiance.*

	Reference	IGVs (+9°)	IGVs (-9°)	VRS 3
[RPM]N_{comp}	46000	46000	46000	42111
[kg/s]$\dot{m}_{corr,comp}$	0.598	0.615	0.55	0.558
R_{comp}	2.80	2.86	2.67	2.58
$\eta_{s,comp}$	0.72	0.74	0.67	0.78
[kW]W_{comp}	82.2	84.4	77.5	64.6
[RPM]N_{turb}	46000	46000	46000	52684
R_{turb}	2.59	2.63	2.47	2.38
$\eta_{s,turb}$	0.85	0.84	0.85	0.88
[K]TIT	1021.5	1000.8	1108.7	983.8
[kW]W_{turb}	124.7	126.9	119.9	106.9
[kW]$\dot{Q}_{solar}$	239.1	241	233.1	254
[kW]$\dot{Q}_{combustion}$	165.8	158.6	203.5	123.8
Solar fraction	0.59	0.60	0.53	0.66

Of the variable rotor speed SHGT configurations, the third system, with independent and distinct compressor and turbine rotor speeds, shows the most marked improvement in performance, with estimated changes in fuel consumption and solar fraction, relative to the reference case, of -25.3 % and 6.6 %, respectively. Substantial shifts are noted in the operating points, including the efficiencies, of both turbomachines. For the first and second variable rotor speed SHGT configurations, respective fuel consumption changes of -18.5 % and -22.8 % are estimated, with values of 4.6 % and 5.8 % estimated for the respective changes in solar fraction.

The performance calculations carried out for 800 W/m² solar irradiance and the same prescribed load of 40 kW_e are noted to yield similar results. For part load operation of the configurations (30 kW_e, 800 W/m² irradiance), the results of the performance calculations show a modest change in fuel consumption of approximately -3.6 % for the SHGT with compressor IGVs set at 9°, compared to the reference case, and a more substantial improvement of -38.5 % for the third variable rotor speeds SHGT configuration. A marked increase is observed when the prescribed load is reduced further to 20 kW_e at 800 W/m² solar irradiance, with estimated changes in fuel consumption of -4.81 % for the SHGT system, and -72.6 % for the third variable rotor speeds configuration. The differences between these results and those previously reported for variable rotor speed SHGT configurations [1] is thought to be due to differences in the sizes and designs of the system components considered in the analyses, as well as the revised optimisation strategy implemented in this work, though this is still to be verified in future.

6. Conclusion

An analysis of the potential performance gains attainable by using compressor inlet guide vanes (IGVs) to facilitate improved component matching in a 40 kW_e solar hybrid gas turbine system (SHGT) is presented. Several SHGT configurations designed for variable rotor speeds are also considered, for comparison. Performance of the SHGTs with IGVs directed towards the direction in which the rotor blades rotate is found to compare favourably to that of the reference system, with a reduction in fuel consumption of 4.3 % calculated for the maximum IGV setting angle of 9° considered in the analysis. A significantly greater reduction of 25.3 % is calculated for the SHGT with independent and distinct compressor and turbine rotor speeds. The performance gains estimated for the compressor IGV- and variable rotor speed configurations are proportionally consistent with their relative levels of technical complexity. These findings are encouraging and warrant similar analyses of differently sized systems and other types of turbomachines to assess the generality of the approaches.

Author contributions

Matthew R. Meas: Investigation, Writing – original draft, **Sybrand J. van der Spuy:** Supervision, Writing – review & editing, **Andrew Gill:** Supervision, Writing – review & editing.

Competing interests

The authors declare that no competing interests have influenced this work.

Acknowledgements

The authors thank the Solar Thermal Energy Research Group (STERG) and South African National Government Department of Higher Education and Training for the funding to partake in the SolarPACES 2024 conference.

References

[1] M. R. Meas, T. W. von Backström, and S. J. van der Spuy, “Performance analysis of variable speed solar gas turbine configurations”, *AIP Conference Proceedings*, vol. 2445, 2022. DOI: https://doi.org/10.1063/5.0086271.
[2] R. V. Luiten, *Performance Improvement of the Rover 1S/60 Gas Turbine Compressor*, master’s thesis, 2015.
[3] R. Aungier, *Centrifugal Compressors: A Strategy for Aerodynamic Design and Analysis* (ASME Press, New York, 2000).
[4] A. L. de Wet, *Performance Investigation of a Turbocharger Compressor*, master’s thesis, 2011.
[5] J. Kurzke, GasTurb 13: Design and Off-Design Performance of Gas Turbines, Manual, (GasTurb GmbH, 2018).
[6] H. I. H. Saravanamuttoo, G. F. C. Rogers, H. Cohen, P. V. Straznicky, and A. C. Nix, *Gas Turbine Theory* (Pearson, 2017), 7th Edition.
[7] P. Gauche, S. Pfenninger, A. J. Meyer, T. W. von Backström, and A. C. Brent, “Modeling dispatchability potential of CSP in South Africa”, in *Proceedings of the first Southern African Solar Energy Conference,* Cape Town, South Africa, 2012.
[8] W. B. Stine and M. Geyer, *Power from the Sun*, 2001. ISBN 0036-8075. Available at: http://www.powerfromthesun.net/book.html
[9] W. G. Le Roux, T. Bello-Ochende, and J. P. Meyer, “The efficiency of an open-cavity tubular solar receiver for a small-scale solar thermal Brayton cycle”, *Energy Conversion and Management*, vol. 84 pp.457–470, 2014. DOI: https://doi.org/10.1016/j.enconman.2014.04.048